Stopping Power Simulation for Use in Muon Tomography

Ishbel Jamieson,[1] Alan D. Bross,[2] E. C. Dukes,[3] Ralf Ehrlich,[3] Eric Fernandez,[3] Sophie Dukes,[4] Mohamed Gobashy,[5] Patrick J. La Rivière,[6] Gregory Marouard,[7] Nadine Moeller,[7] Anna Pla-Dalmau,[1] Paul Rubinov,[1] Omar Shohoud,[8] Phillip Vargas,[6] and Tabitha Welch[8]

[1]*Department of Physics, University of Oxford, Oxford, UK*
[2]*Fermi National Accelerator Laboratory, P.O. Box 500, Batavia, IL, USA*
[3]*Physics Department, University of Virginia, Charlottesville, VA, USA*
[4]*Virginia Tech University, Blacksburg, WV, USA*
[5]*Geophysics Department, Faculty of Science, Cairo University, Cairo, Egypt*
[6]*Department of Radiology, University of Chicago, Chicago, IL, USA*
[7]*Department of Near Eastern Languages & Civilizations Yale University, New Haven, CT, USA*
[8]*Department of Physics, University of Chicago, Chicago, IL, USA*

Corresponding author: Ishbel Jamieson
Email: ishbel.jamieson@gmail.com

Abstract

The field of muon tomography has developed rapidly over recent years. It has seen broad-ranging applications, from archaeology to nuclear waste management. The technique relies upon the varying attenuation of muons passing through materials, parameterized by the stopping power—the energy lost by the muon per unit distance traveled—and is intrinsic to the material itself. As this is an inverse problem, it is important that the reconstruction is particularly sensitive to this function to correctly identify the material itself. It is the aim of this paper to outline an efficient, closed-form simulation of the stopping power for compound materials that, by design, allows for user-friendly application to most materials.

Keywords: stopping power, muon tomography
DOI: 10.31526/JAIS.2022.281

1. INTRODUCTION

The tomographic reconstruction of a large structure or object requires a mapping between the number of muons detected, expressed as a flux, and the density of the path traversed by the binned muon direction, expressed as opacity. The binning of the muon directions is largely independent of the calculation of the stopping power and will not be covered in any great detail. However, for clarity, it refers to a ray within a certain positional bin on the detection plane (determined by the resolution of the detector) and an angular bin, determined by the binning regime—which is specific to the geometry and aims of a project. The relationship between flux and opacity is outlined by a set of relatively simple equations given below.

We start with the definition of opacity: a line integral along the binned muon direction.

$$\varrho\left(x_i, z_j, \theta_k, \phi_m\right) = \int_{L(x_i, z_j, \theta_k, \phi_m)} \rho(x, y, z) dl, \tag{1}$$

where ϱ is the opacity, $(x_i, z_j, \theta_k, \phi_m)$ are the bin's parameters, and $\rho(x, y, z)$ is the density of the material at position $(x, y, z)t$.

As muon tomography generally explores density variations within a solid structure, a homogeneous baseline model is used to compare experimental results. For a homogenous material, our definition of opacity reduces to:

$$\varrho = \rho L, \tag{2}$$

where L is the path length and ρ is now a constant. With this linear relationship in L, we can model it to be the mean range—the average distance traveled by the muon before coming to rest—while working in the continuous slowing down approximation (CSDA) [1]. By scaling the definition of the mean range by density, we produce the following expression for the maximum opacity that can be traversed b a muon of energy E_{min}:

$$\varrho = \int_0^{E_{\text{min}}} \frac{1}{\frac{dE}{d\varrho}} dE. \tag{3}$$

Here, $\frac{dE}{d\varrho}$ is the mass stopping power of the material. For a homogeneous model, this reduces simply to $\frac{dE}{dx}$ and a density coefficient (as explained above), with $\frac{dE}{dx}$ being the stopping power of the material, and the subject of this paper. It is a function of energy alone and is given by the following equation:

$$\left\langle -\frac{dE}{dx} \right\rangle = a(E) + b(E) \cdot E. \tag{4}$$

Here, we can see that it is comprised of two types of processes that result in energy loss: $a(E)$ that accounts for the electronic interactions and $b(E)$, which accounts for several radiative processes. For a compound such as the limestone in the Great Pyramid, this becomes a mass-weighted average of individual elemental constituents:

$$\frac{dE_{\text{compound}}}{dx} = \sum_j q_j \frac{dE_j}{dx}, \tag{5}$$

where q_j is the mass fraction of the j^{th} element in the compound. As such, given a fractional breakdown of a compound's make-up, the stopping power of any material may be readily calculated.

2. ENERGY RANGE

This particular simulation was developed under the Exploring the Great Pyramid (EGP) collaboration and, therefore, the following energy limits are specific to the project—the considerations are, however, general to the technique of muon tomography.

The Daya-Bay model of the muon flux incident at sea level, a modified form of the Gaisser formula, was used for its ability to better describe the spectrum at lower energies (below 100 GeV) [2].

By considering the Daya-Bay model of the muon flux incident on the Earth's surface, we can see a severe energy dependence.

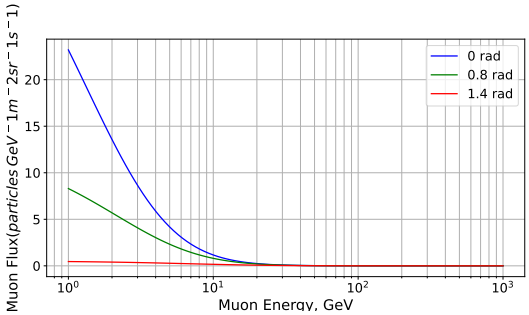

FIGURE 1: The Daya-Bay model of the muon energy spectrum at sea level, for a number on angles.

Due to the positioning of the detectors and the geometry of the Pyramid, most rays with a zenith angle below 45° (around 0.8 rad) will be thrown out in the reconstruction process as they typically will not have passed through the pyramid.

We may observe the sharp drop in muon flux as the energy increases, though much less so for the angles we are considering, which at around 1 TeV becomes almost negligible. 1 TeV is the upper limit of the energies considered in this project. The lower limit is largely dictated by the minimum distance a muon must pass through the pyramid for it to be accepted in the reconstruction code. The minimum energy associated with this distance was found to be around 30 GeV, which set the lower limit for the energy considerations. It can be seen from Figure 1 that the lower energy muons are the greatest contributors to the integrated flux and so it is necessary to set the lower limit to be such that a sufficient number of muons are still being considered in the reconstruction process to produce a high-resolution image.

3. CONTRIBUTIONS TO STOPPING POWER

As seen earlier, the contributions to stopping power may be split into two types of processes: electronic and radiative. They are broken down as follows:

$a(E)$: Bethe-Bloch,
$b(E)$: Bremsstrahlung, pair production, and photonuclear interactions.

At low energies, below 100 GeV, the electronic processes dominate this energy loss, and above this, the radiative processes dominate. Since our energy range bridges both limits, the two types must be considered with equal importance.

3.1. *Bethe-Bloch Equation*

The well-known Bethe-Bloch equation accounts for the energy loss a charged particle experiences as it ionizes or excites the atoms in the material [3]. Two additional higher-order corrections have been included in the code:

(1) Bremsstrahlung from atomic electrons: this significantly contributes to the total electronic losses, particularly at higher energies (4% at 1 TeV) [4].
(2) Barkas-effect correction: this approximation holds in our energy range; however, fails above 2 TeV [5].

As concrete is a compound material, with both conductive and nonconductive constituents, as well as having a wealth of existing data on the popular grades, it was chosen as the test compound for the final simulation.[1] From these constituents, silicon was then chosen for its second highest mass fraction (being 0.337 compared to Oxygen with 0.529). Shown below, in Figure 2, is the result of implementing the Bethe-Bloch equation in the code, along with the chosen corrections, for silicon:

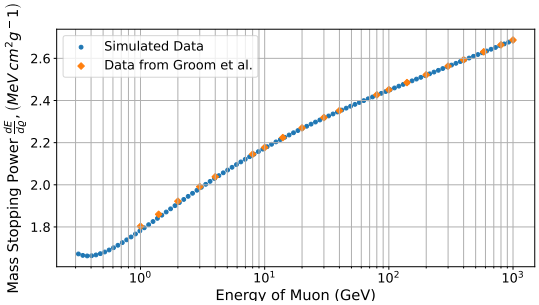

FIGURE 2: The contribution of electronic processes to the mass stopping power of silicon.

They have been compared against the data produced by Groom, Mokhov, and Striganov, 2001 [7] (shown above) as well as with existing Geant4 simulations for silicon [8]. Due to the simple nature of this formulation of the Bethe-Bloch equation, the code took 1.1507 seconds to produce the results in Figure 2.

3.2. *Bremsstrahlung*

Bremsstrahlung is the radiation emitted as the muon is deflected by the electrons and atomic nuclei of the material, resulting in a deceleration of the muon. Kelner, Kokoulin, and Petrukhin's 1995 paper on Bremsstrahlung cross-section for high-energy muons [9] has been used here. Not only are numerous significant corrections included, but they also have a concise breakdown of the history of Bremsstrahlung formulations.

Shown below is the result of implementing these corrections in the code.

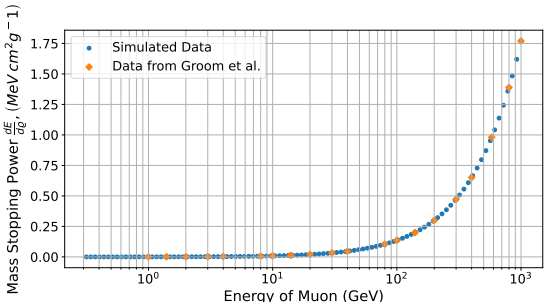

FIGURE 3: The contribution of Bremsstrahlung to the mass stopping power for silicon.

3.3. *Pair Production*

The production of e^+e^- pairs results from the electromagnetic interactions of the muon as it passes through the material. There have been several formulations of this, the most recent being Nikishov's analytic form for the energy spectrum of the pairs produced [10]. Though thorough, this form greatly reduced the efficiency of the code due to its length. Therefore, the use of Kokoulin and Petrukhin's parameterization of Kelner and Kotov's was more appropriate [11, 12]. Shown below are the results of this.

[1] More specifically, Portland concrete was chosen [6].

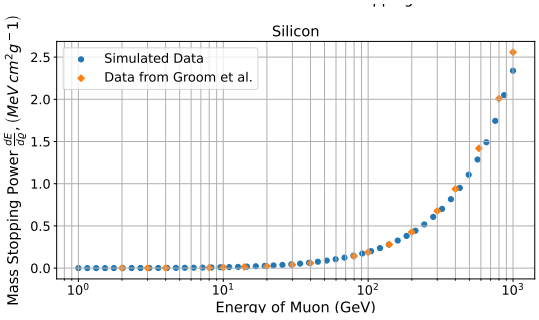

FIGURE 4: The contribution of pair production to the mass stopping power of silicon.

3.4. Photonuclear Interactions

The energy loss due to photonuclear interactions is the product of multiple complex processes. The most popular form is that formulated by Bezrukov and Bugaev [13] in 1981, still widely used today.

There is, however, a problem—this approximation fails for energy losses below 5 GeV. Since the method relies upon an integration over the fractional energy transfer, this limits the accuracy of this method around the lower limit of our energy range.

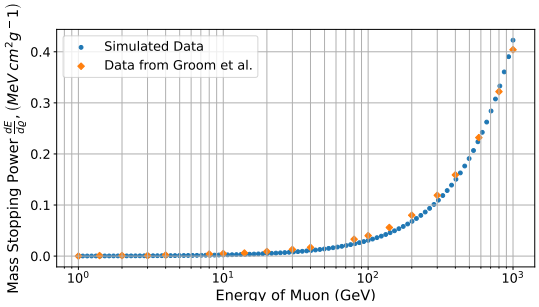

FIGURE 5: The contribution of photonuclear interactions to the mass stopping power of silicon.

4. INPUT AND RESULTS

The final code itself takes a csv file as its input—easily produced and edited in Excel. Shown in Figure 6 is a simplified extract of this csv file for concrete.

	Hydrogen	Carbon	Oxygen	Sodium	Magnesium
Mass Fraction	0.01	0.001	0.529107	0.016	0.002
Atomic Number (Z)	1	6	8	11	12
Atomic Mass (A)	1.008	12.011	15.999	22.98977	24.305
Mean Excitation Energy (eV)	19.2	78	95	149	156

FIGURE 6: A simplified extract of the input for concrete.

The results for an individual constituent took on average 13 minutes, 10 minutes of which was taken up by the code for pair production, setting a total of 130 minutes for the final stopping power of concrete.

Drawing all of the above processes together, we produce the total stopping power shown below in Figure 7. From this, we observe that the results of the code agree very well with the existing results obtained by Groom et al. [7], particularly for energies below 100 GeV—useful as these.

There are also several ways in which the pair production may be edited to further cut the run-time:

(1) Decrease the sampling rate for the numerical integrations involved—not advisable due to the rapidly changing fractional energy transfer.
(2) Reduce the number of energy sample points and instead interpolate the data for use in the final result—preferred over the above as the functional form of pair production (in Figure 4) is relatively standard, so it can be simply modeled for interpolation.

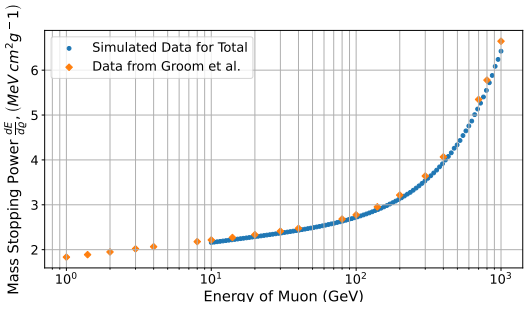

FIGURE 7: The final stopping power function produced.

5. CONCLUSION

The results of the closed-form analysis of the stopping power are congruent with existing literature and are therefore a promising simulation for a compound material. Qualitative breakdowns of the Great Pyramid's backing block constituents exist [14], and a quantitative breakdown will be helpful for use in the EGP collaboration in order to achieve the intended full precision of this method. As it stands, however, the specialized nature of the code and the ease of custom input make it an efficient candidate for the use in muon tomography.

CONFLICTS OF INTEREST

The authors declare that there are no conflicts of interest regarding the publication of this paper.

ACKNOWLEDGMENTS

I am deeply grateful for the continued support of Prof. Todd Huffman, Dr. Anne Mullen, and the faculty of Lady Margaret Hall—all of whom have made this possible. This document was prepared using the resources of the Fermi National Accelerator Laboratory (Fermilab), a U.S. Department of Energy, Office of Science, HEP User Facility. Fermilab is managed by Fermi Research Alliance, LLC (FRA), acting under Contract No. DE-AC02-07CH11359.

References

[1] J. C. Ashley, C. J. Tung, R. H. Ritchie, and V. E. Anderson. Inverse mean free path, stopping power, CSDA range, and straggling in Ge and GaAs for electrons of energy 10 keV. Interim Report, November 1976.
[2] Guan Mengyun, Cao Jun, Yang Changgen, Sun Yaxuan, and Kam-Biu Luk. Muon simulation at the daya bay site.
[3] H. Bethe. Theory of the Passage of Fast Corpuscular Rays Through Matter. *Annalen Phys.*, 5: 325–400, 1930.
[4] Alexander Sandrock, Stanislav R. Kelner, and Wolfgang Rhode. Radiative corrections to the average bremsstrahlung energy loss of high-energy muons. *Phys. Lett. B*, 776: 350–354, 2018.
[5] J. D. Jackson and R. L. McCarthy. z^3 corrections to energy loss and range. *Phys. Rev. B*, 6: 4131–4141, Dec. 1972.
[6] NIST. Composition of concrete, Portland.
[7] Donald E. Groom, Nikolai V. Mokhov, and Sergei I. Striganov. Muon stopping power and range tables 10 MeV–100 TeV. *Atomic Data and Nuclear Data Tables*, 78(2): 183–356, 2001.
[8] S. Banerjee, Alessandra Caner, Suchandra Dutta, Alexandre Khanov, Fabrizio Palla, and G. Tonelli. Silicon Bethe Bloch muon (GEANT) proton (GEANT) electron (GEANT) $\beta\gamma$. 2007.
[9] S. R. Kelner, R. P. Kokoulin, and A. A. Petrukhin. About cross section for high-energy muon bremsstrahlung. Technical report, Aug 1995.
[10] A. I. Nikishov. Energy Spectrum of e+ e- Pair Created in Muon Collision with an Atom. *Sov. J. Nucl. Phys.*, 27: 677, 1978.
[11] R. P. Kokoulin and A. A. Petrukhin. Analysis of cross section of direct pair production by fast muons. *Acta Phys. Acad. Sci. Hung. 29: Suppl. 4, 277–284 (1970).*
[12] S. R. Kelner and Yu. D. Kotov. *Sov. J. Nucl. Phys.*, 7: 237, 1968.
[13] L. B. Bezrukov and E. V. Bugaev. Nucleon shadowing effects in photonuclear interactions. *Sov. J. Nucl. Phys. (Engl. Transl.); (United States).*
[14] Sayed Hemeda and Alghreeb Sonbol. Sustainability problems of the giza pyramids. *Heritage Science*, 8: 8, 01 2020.